Phase-speed Spectra of Eddy Tracer Fluxes Linked to Isentropic Stirring and Mixing in the Upper Troposphere and Lower Stratosphere

MARTA ABALOS AND WILLIAM J. RANDEL

National Center for Atmospheric Research,[a] *Boulder, Colorado*

THOMAS BIRNER

Department of Atmospheric Science, Colorado State University, Fort Collins, Colorado

(Manuscript received 2 June 2016, in final form 22 September 2016)

ABSTRACT

The regions around the subtropical jets in the upper troposphere and lower stratosphere (UTLS) are characterized by strong isentropic stirring and mixing. In this work, the wave spectrum of the associated eddy tracer fluxes is examined using an artificial passive tracer advected on isentropes by the two-dimensional flow. The eddy diffusivity computed from the flux–gradient relation captures the main features of the mixing structure. Eddy transport in the UTLS is strongest in the summer hemisphere, and weak eddy fluxes are found at the core and poleward of the subtropical jets, especially in the winter hemisphere. There is an important contribution of stationary planetary equatorial Rossby waves in the tropical upper troposphere. The transient eddy tracer transport is primarily linked to medium-scale waves (wavenumbers ~4–7) breaking in the regions of weak westerlies around the subtropical jets and to planetary-scale waves at high latitudes. Phase-speed spectra for transient eddy fluxes show a close relationship of waves to the background zonal wind. In the deep tropics, traveling equatorial and Rossby waves of extratropical origin lead to cross-equatorial tracer transport throughout the upper troposphere. Interannual changes show that eddy tracer fluxes closely follow the shifts in the zonal winds associated with El Niño–Southern Oscillation and the quasi-biennial oscillation.

1. Introduction

The effective diffusivity calculations in Haynes and Shuckburgh (2000a,b) and Allen and Nakamura (2001), and more recently in Abalos et al. (2016), show strong isentropic mixing around the subtropical jets, as well as in the stratospheric surf zone. These analyses are based on a passive tracer transported in two dimensions (2D) by the nondivergent part of the reanalysis isentropic winds and provide an accurate and robust measure of mixing structure and strength (Shuckburgh and Haynes 2003; Nakamura 2008). The isentropic stirring of a tracer is associated with the dissipation of Rossby waves as they reach their critical lines, determined by their spatial and temporal scales and the background flow (Charney and Drazin 1961; Matsuno 1970). Wave breaking leads to deformation of the tracer contours and formation of long filamentary structures stripped away from their originating region that ultimately get mixed with the surrounding air (McIntyre and Palmer 1983).

By analyzing the evolution of the passively advected tracer used for the effective diffusivity calculations in Abalos et al. (2016), in the present work we examine the underlying waves leading to isentropic mixing. The passive tracer is advected in 2D by the nondivergent part of the isentropic wind, which satisfies $\nabla \cdot \mathbf{u} = 0$, where $\mathbf{u}$ is the wind field on the isentropes. This choice of the nondivergent wind field implies that we assume layer-wise 2D barotropic dynamics. This approach has been followed in several previous studies of 2D isentropic transport (e.g., Waugh et al. 1994; Haynes and Shuckburgh 2000a,b; Allen and Nakamura 2001). The use of nondivergent winds is motivated by the need to adapt the inherently 3D reanalysis wind field into a purely two-dimensional circulation. Although the rotational flow dominates in the extratropics, the divergent

[a] The National Center for Atmospheric Research is sponsored by the National Science Foundation.

Corresponding author address: Marta Abalos, National Center for Atmospheric Research, P.O. Box 3000, Boulder, CO 80307-3000.
E-mail: abalos@ucar.edu

DOI: 10.1175/JAS-D-16-0167.1

© 2016 American Meteorological Society. For information regarding reuse of this content and general copyright information, consult the AMS Copyright Policy (http://www.ametsoc.org/PUBSCopyrightPolicy).

flow represents a nonnegligible component of the total wind field in the tropical troposphere, and thus our results in this region need to be interpreted more cautiously. A fundamental advantage of the 2D barotropic dynamics considered here is that the tracer continuity equation is simply

$$\overline{\chi}_t = -(\overline{v_r'\chi'})_y + \overline{S}, \tag{1}$$

where v_r is the rotational component of the meridional wind, subscripts indicate partial derivatives, the overbar indicates zonal mean, and the primes are deviations from it. Note that the zonal-mean advective term of the tracer continuity equation ($-\overline{v}_r\overline{\chi}_y$) is zero and thus not included in Eq. (1). This is because the rotational part of the wind is derived from a streamfunction ($v_r = -\Psi_x$) and thus is zero in the zonal mean. Since there are no sources or sinks for the passive tracer by definition, the term $\overline{S}$ in Eq. (1) includes only numerical diffusion. In practice, this term is small and the zonal-mean tracer tendency is balanced by the eddy transport term in Eq. (1), which is linked to two-way mixing (not shown).

Here we investigate the space–time spectral characteristics of the 2D barotropic tracer transport using the meridional eddy tracer flux ($\overline{v_r'\chi'}$). Abalos et al. (2013) analyze the waves associated with the eddy transport of ozone in the tropical lower stratosphere by computing the phase-speed spectrum of the eddy ozone flux (at one specific level and season). The phase-speed spectrum as a function of latitude was introduced by Randel and Held (1991) to analyze dynamical eddy fluxes in the troposphere and has been subsequently used in a number of works to examine the phase-speed decomposition of the waves in relation to the background flow (e.g., Kim and Lee 2004; Chen and Held 2007; Chen et al. 2008; Shepherd and McLandress 2011). This diagnostic allows one to relate the phase speed of the waves to the background flow and provides useful insights on the eddy fluxes and associated transport.

Previous work has focused on analysis of potential vorticity (PV) fluxes, which are similar in several respects to conservative tracer fluxes. The PV of an air parcel is conserved in adiabatic frictionless flows, and thus PV is frequently used as a material tracer in transport studies, assuming that sources and sinks are negligible (e.g., Waugh and Plumb 1994). However, this conservation is not satisfied in regions of strong diabatic heating. On the other hand, for adiabatic conditions the isentropic eddy PV flux equals the divergence of the Eliassen–Palm flux such that it quantifies the eddy–mean flow dynamical interactions (e.g., Hoskins et al. 1985; Tung 1986). Here we compute the eddy fluxes for a passively transported tracer conserved on isentropic surfaces, and we include some comparisons with PV flux when relevant.

The aim of this work is to examine the characteristics of the waves responsible for the mixing structure and seasonality obtained from effective diffusivity calculations. In section 2, we introduce the artificial tracer and describe the calculations. Section 3 provides a first description of the eddy fluxes, separating planetary- from medium-scale waves, and transient from stationary waves. Section 4 presents the phase-speed spectra decomposition on some key levels in the upper troposphere and lower stratosphere (UTLS). Section 5 briefly explores interannual variability in the eddy tracer fluxes.

2. Data and calculations

a. *Artificial tracer*

The analyses are based on an artificial passive tracer transported on isentropes using the advection–diffusion model described in Haynes and Shuckburgh (2000a,b) and more recently in Abalos et al. (2016). As in the latter work, we use the 6-hourly isentropic winds from ERA-Interim as input (Dee et al. 2011). Only the nondivergent part of the wind is used in order to have consistent two-dimensional dynamics. The model has a resolution-dependent diffusivity parameter, which is set to $\kappa = 10\,474\,\mathrm{m^2\,s^{-1}}$ for the T255 ERA-Interim data used here. This numerical diffusivity is necessary to damp structures smaller than the grid of the input data [refer to Abalos et al. (2016) for further information on the choice of the diffusivity parameter]. In this work the artificial tracer is initialized as a linear function of latitude [$\chi = -\phi/(\pi/2)$] on each isentropic level. This monotonic initialization ensures uniform gradients at all latitudes such that the strength of the eddy fluxes is not biased by steeper initial tracer gradients in some regions. We note that, although this initialization differs slightly from that used in Abalos et al. (2016), which was $\chi = -\sin\phi$, the effective diffusivity is the same for any tracer initialization as long as it is monotonic (Haynes and Shuckburgh 2000a). We consider the two solstice seasons: December–February (DJF) and June–August (JJA). The tracer is initialized 1 month prior to the start of each season (first day of November and first day May, respectively) and advected for 4 months. The first month is used to allow the tracer to align with the flow and is not considered in the analyses. The calculations have been done for all years in the 1980–2014 period in the ERA-Interim dataset and on a set of 29 isentropic levels spanning the UTLS (300–800 K). The spacing between the levels is 10 K in the layer 300–500 K, 25 K in the

layer 500–600 K, and 50 K in the layer 600–800 K. The cross sections in this work are shown as a function of log-pressure altitude for visualization purposes to emphasize the UTLS region, but all the analyses are carried out on isentropic levels, and the zonal-mean quantities are interpolated to log-pressure levels (using a scale height of 7 km) as a last step just before plotting.

Figures 1a and 1c show the evolution of the artificial tracer concentrations on the 400-K level during DJF and JJA averaged over all years. The tracer rapidly spreads from low to high latitudes in the summer hemisphere at this level, and the meridional gradients are substantially reduced over time [this spread is faster in the Northern Hemisphere (NH) summer than in the Southern Hemisphere (SH) summer]. In the winter hemisphere there is a notably slower progression of the tracer contours toward high latitudes, and the meridional gradients remain strong throughout the season. Note that the tracer in the deep tropics shows a narrowing of the contours during approximately the first two weeks to allow the contours, initially parallel to latitude circles, to adjust to the wind structure.

Figures 1b and 1d show the global structure of the tracer averaged over the entire season for DJF and JJA. The summer lower stratosphere is highlighted as a region of particularly wide spread of the tracer contours and weakened meridional gradients, with tropical values of the tracer reaching high latitudes (as seen in Figs. 1a,c). This behavior is observed over a layer of ~5 km approximately around the 400-K isentrope in both hemispheres (stronger in the NH). Largely homogenized concentrations in the summer lower stratosphere are also found in tracer observations (e.g., Hegglin and Shepherd 2007; Bönisch et al. 2009; Ploeger et al. 2013). In the winter hemisphere there is some evidence of isentropic mixing above the subtropical jet as well, but it is much weaker than in the summer hemisphere.

In the stratosphere, above ~20 km, the tropical pipe (Plumb 1996) is easily identified by the strong meridional gradients of the tracer equatorward of ~30°N/S, indicating weak mixing. The bottom of the tropical pipe is found around 400 K. The polar vortex in the winter stratosphere acts as a barrier maintaining strong gradients across its jet core. The stratospheric surf zone (McIntyre and Palmer 1983) can be observed as a region of spread-out tracer contours equatorward of the vortex edge in the winter hemisphere. The summer stratosphere of both hemispheres shows relatively uniform concentrations in high latitudes, clearly distinguished from the tropical region. This could be linked to breaking westward-traveling waves in the summer stratosphere, studied by Wagner and Bowman (2000). The subtropical jet cores act as barriers for transport, as evidenced by the strong tracer meridional gradients across them, especially in the winter hemisphere. In the tropical upper troposphere the tracer gradients are much weaker than in the tropical stratosphere, indicating stronger isentropic mixing within this region. We note that the tracer distribution in Figs. 1b and 1d is overall consistent with that obtained by Chen and Plumb (2014) using a model with full three-dimensional transport, at least for the first 90 days (cf. their Fig. 4, left column). This implies that the isentropic component of transport accounts for a large fraction of the total transport on these time scales. The main differences are found below 500 hPa in the deep tropics, where fast vertical motions dominate in the full three-dimensional transport model (and in the real atmosphere). The idealized Lagrangian transport calculations of Bowman and Carrie (2002) also highlight isentropic transport dominating tropospheric transport outside the deep tropics.

b. *Eddy tracer flux phase-speed spectra*

As discussed in the introduction, the artificial passive tracer advected on isentropes by the nondivergent component of the wind satisfies the simple transport equation [Eq. (1)], and we have verified that the term $\overline{S}$, computed as a residual, is negligible. This implies that numerical diffusion does not play an important role in the balance, and thus the tracer tendency is driven by eddy transport. In the rest of the paper we analyze the isentropic eddy tracer flux $\overline{v_r'\chi'}$.

We follow Randel and Held (1991) in computing the phase-speed spectra of the transient eddy tracer flux as a function of latitude. For each season and latitude, the space–time cospectrum is calculated for the eddy flux:

$$\mathrm{CO}_{\omega,k} = 2\langle \mathrm{Re}(A_{\omega,k} B^*_{\omega,k}) \rangle, \tag{2}$$

where $A_{\omega,k}$ and $B_{\omega,k}$ represent the Fourier transform components in time and longitude of the meridional wind and the tracer concentration for a given frequency ($f = \omega/2\pi$) and wavenumber ($\mathrm{wn} = ka\cos\phi$, with a being Earth's radius and ϕ being the latitude), and the asterisk indicates the complex conjugate. The angle brackets represent an average over different years. To reduce the effect of spectral leakage due to the finite 90-day time series, we taper the series with a Hanning window. We construct daily mean time series from the 6-hourly data, such that the minimum period resolved is 2 days (Nyquist frequency of 0.5 cycles per day). This is done to reduce data storage requirements, and we have checked that there is no significant loss of information as a result (there is small spectral power in the range 0.25–1 day). Note that the effect of aliasing by time scales shorter than a day is small, because we use daily mean

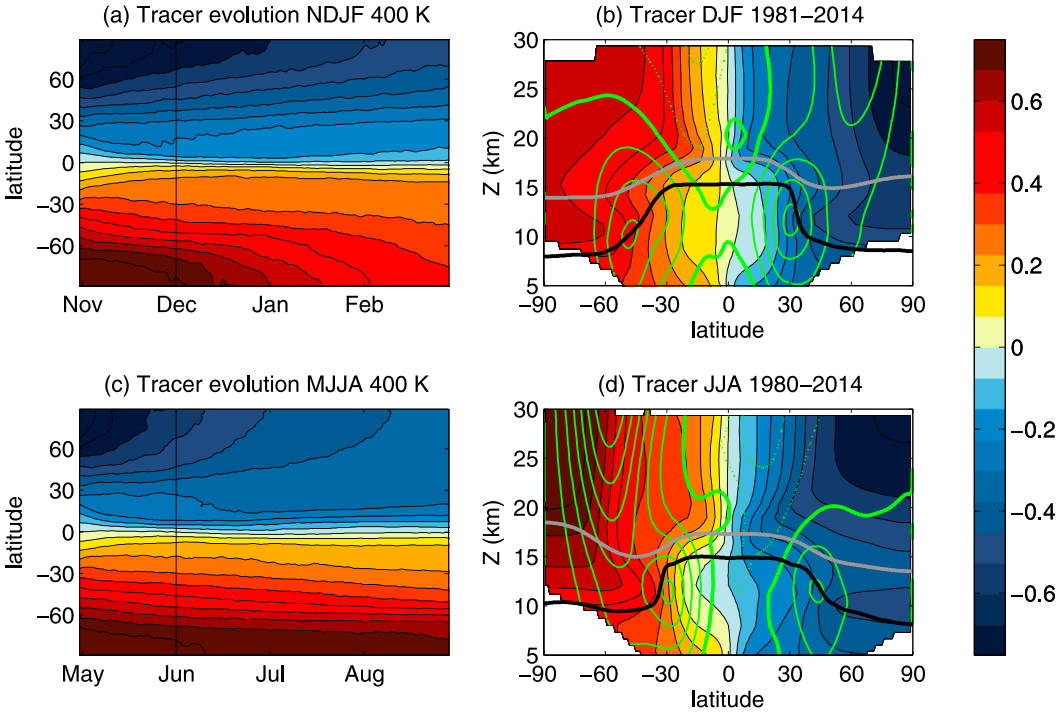

FIG. 1. (left) Artificial tracer evolution at 400 K as a function of latitude for (a) November–February and (c) May–August. The first month is not considered in the calculations (see text for details). (right) Artificial tracer seasonal-mean latitude–altitude cross section for (b) DJF and (d) JJA. Green contours show the zonal-mean wind with a 10 m s^{-1} spacing (thin solid for positive, dotted for negative, thick solid for zero). The gray contour shows the level of 400 K, and the black contour shows the lapse-rate tropopause for the seasonal mean. The units of the artificial tracer are arbitrary.

data computed from 6-hourly reanalysis data, so only time scales under 6 h can produce aliasing. The co-spectrum $CO_{\omega,k}$ is then expressed as a function of the phase speed $c = \omega/k$, ensuring the conservation of total power $CO_{c,k} = kCO_{\omega,k}$. The results are then summed over zonal wavenumber and shown as a function of latitude for different bands of wavenumbers in section 4.

3. Eddy tracer flux

a. Relation between eddy flux and isentropic mixing

Figures 2a and 2c show the eddy tracer fluxes averaged over all years for the two seasons considered. The eddy tracer flux is positive everywhere, which implies a downgradient flux, given the background latitudinal tracer gradient. There are large values of the eddy flux above and below the subtropical jets, in the tropical upper troposphere, and in the stratospheric surf zone at the edge of the polar vortices. The fluxes above the subtropical jets extend farther poleward in the summer hemisphere, while in winter hemisphere they are limited to lower latitudes by the stronger winds in the upper flank of the jet. The lower part of the polar vortices further contributes to limit the extent of the eddies in the winter lower stratosphere. For instance, in the SH winter (JJA) there are particularly weak fluxes poleward of the subtropical jet in the layer ~10–15 km. There are weak eddy fluxes at the subtropical jet cores and poleward of the jets, especially in the winter hemisphere. This is consistent with the role of the jets as transport barriers for two-way mixing. The features in Figs. 2a and 2c are highly consistent with the tracer distribution in Fig. 1 and with the simple balance in Eq. (1).

Figures 2b and 2d show the corresponding eddy PV fluxes (computed with the full meridional wind). Strong similarities are observed between tracer and PV fluxes (with sign changed due to the opposite-sign meridional gradients of PV and the tracer). Important exceptions are found near the core of the subtropical jets in both hemispheres and in the upper troposphere near the equator, where the PV fluxes show positive values. Birner et al. (2013) showed that the positive PV fluxes near the core of the winter subtropical jets correspond to upgradient fluxes related to finite-amplitude effects (nonnegligible PV variance fluxes). The other regions with positive PV fluxes are the tropical upper troposphere near the equator and the region near the core of the

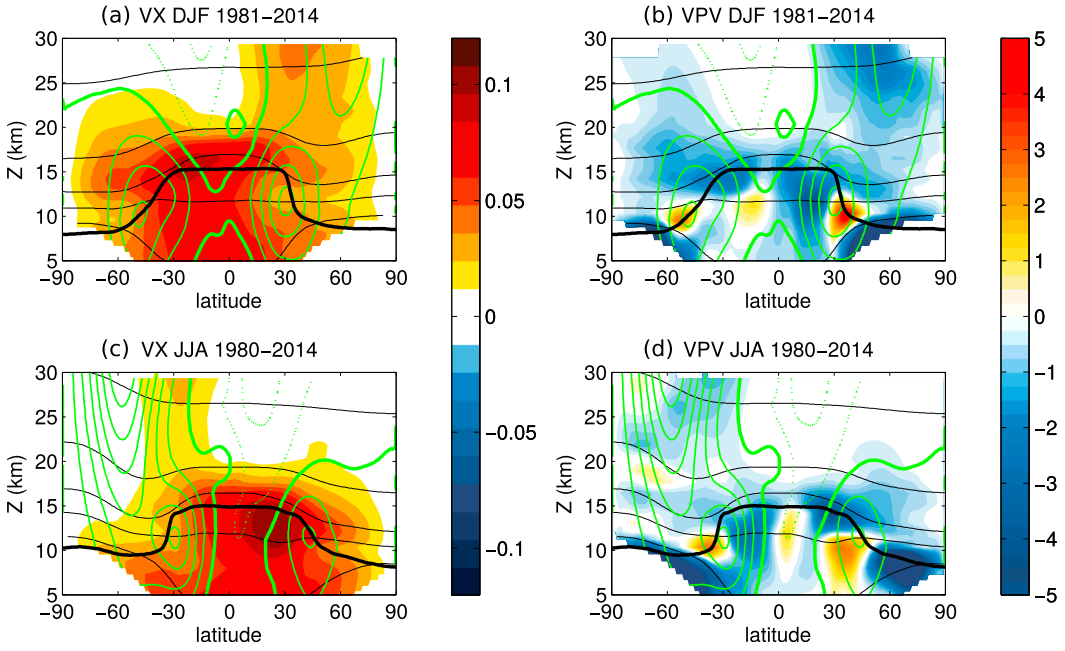

FIG. 2. (left) Eddy tracer fluxes ($\overline{v_r'\chi'}$; m s^{-1}) for (a) DJF and (c) JJA. (right) PV eddy fluxes ($\overline{v'\mathrm{PV}'}$; PVU m s^{-1} = K kg^{-1} m^3 s^{-2}) for (b) DJF and (d) JJA. All fluxes are averaged over 1980–2014. The black contours show isentropes 320, 350, 380, 450, and 650 K. The green contours show the zonal-mean wind with a 10 m s^{-1} spacing (thin solid for positive, dotted for negative, thick solid for zero). The black contour shows the lapse-rate tropopause. VX indicates the eddy tracer flux ($\overline{v_r'\chi'}$).

summer subtropical jet. These positive PV flux values are linked to diabatic sources, in particular the equatorial fluxes are consistent with diabatic generation of quasi-stationary equatorial waves by deep convection (e.g., Randel et al. 2008). The overall similar behavior of the PV and the artificial tracer in Fig. 2 is a manifestation of the near conservation of PV along material lines on isentropic surfaces, and the differences arise mainly from exceptions to this conservation.

We next evaluate the relation between the eddy tracer fluxes and the strength of the mixing, based on the flux–gradient relation (e.g., Plumb and Mahlman 1987; Garcia 1991):

$$K_{yy} = -\frac{\langle \overline{v_r'\chi'} \rangle}{\langle \overline{\chi}_y \rangle}. \tag{3}$$

In this equation the denominator is the zonal mean meridional tracer gradient, and the angle brackets indicate averages over time. Figures 3a and 3c show the climatology of the eddy diffusivity K_{yy} using a time-averaging window of one season (three months). The eddy diffusivity is compared in Fig. 3 to the climatology of the effective diffusivity for each season. The effective diffusivity is a Lagrangian measure of mixing strength that uses a tracer-based system of coordinates [see Abalos et al. (2016) and references therein for further description of these calculations]. Here we use it to verify the validity of the Eulerian estimate [Eq. (3)], which further allows calculating the spectral decomposition of the eddy fluxes. The simplified estimate of mixing, K_{yy}, shows overall good agreement with the structure of mixing as represented by the effective diffusivity (Figs. 3b and 3d). The relatively small differences are due to the different Eulerian versus Lagrangian approaches of the eddy diffusivity versus effective diffusivity estimates. For instance the use of regular latitude instead of equivalent latitude in the zonal mean calculations results in a noisier K_{yy} around the polar vortices, especially in the NH where the vortex position relative to the pole is highly variable. In addition, eddy diffusivity shows very large values in some regions that are not observed in the effective diffusivity (such as the SH stratosphere in DJF or the tropical upper troposphere). Some of these differences might be due to reversible eddy transport, not included in the effective diffusivity. Besides these differences, there is good agreement between these two measures of mixing, both in the structure and the magnitude. This similarity provides strong support to our approach of using the eddy fluxes to analyze the waves underlying the stirring in the UTLS.

b. *Stationary/transient eddies and wavenumber decomposition*

Figure 4 shows the eddy tracer flux $\overline{v_r'\chi'}$ decomposed into its stationary and transient contributions. We have

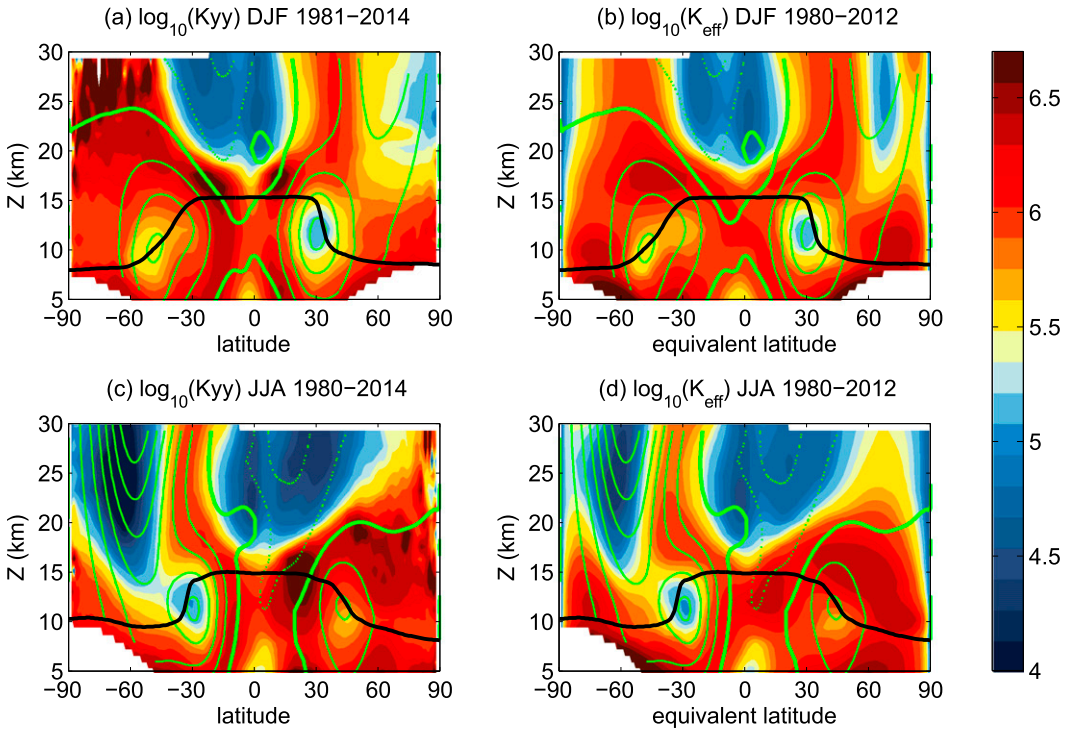

FIG. 3. (left) Eddy diffusivity (K_{yy}; $m^2\,s^{-1}$) computed from eddy tracer flux [Eq. (3)] for (a) DJF and (c) JJA. (right) Effective diffusivity (κ_{eff}; $m^2\,s^{-1}$) for (b) DJF and (d) JJA. The green contours show the zonal-mean wind with a 10 m s^{-1} spacing (thin solid for positive, dotted for negative, thick solid for zero). The black contour shows the lapse-rate tropopause. Note the logarithmic contour scale.

computed stationary waves from the monthly mean fields (and subsequently averaged over the season in Fig. 4) and transient eddies as the difference of the total flux minus the stationary flux. Similar results are obtained computing the stationary component as the seasonal-mean eddy flux, implying little impact of considering time scales between 1 and 3 months as transients. For both seasons the fluxes due to stationary waves are found to be predominant in the tropical upper troposphere and lowermost stratosphere (below ~18 km) and in the winter stratosphere. There is additional evidence of large stationary eddy fluxes in the tropical lower troposphere visible near 5 km, possibly linked to the circulation around subtropical highs. There is a maximum in stationary eddy flux in the NH subtropics during JJA, tied to the Asian monsoon circulation (shown below). The fluxes extending above and below the subtropical jets and in the extratropical UTLS are dominated by transient waves, and there is also a narrow band around the equator characterized by relatively strong transient eddy fluxes. Note that at the core of the boreal winter stratospheric polar jet, the positive stationary eddy fluxes exceed the weaker negative transient eddy fluxes, which results in net weak positive fluxes in this region (weaker than those in the surf zone; see also Figs. 2a,c). Positive transients in the polar night jet are also observed in the PV flux [see for example, the Eliassen–Palm flux divergence in Fig. 3 of Shepherd and McLandress (2011)]. This feature is not observed in the SH polar vortex, where both transient and stationary eddy fluxes are limited to the surf zone. The NH polar vortex is frequently subject to strong perturbations linked to Rossby wave breaking events (including those associated with sudden stratospheric warmings). Stationary planetary-scale Rossby waves in the NH polar stratosphere often lead to displacements of the polar vortex away from the pole, leading to downgradient PV (and tracer) fluxes. As these waves break, transient eddies and associated upgradient fluxes are generated. Maps of the tracer around the dates of strong negative transient eddy fluxes around 60°N show filaments previously stripped from the vortex being wrapped around toward high latitudes (not shown).

Figure 5 decomposes the total eddy flux into planetary-scale (wn = 1–3) and medium- to synoptic-scale (wn = 4–12) wave contributions. As expected from the Charney–Drazin theorem, only planetary-scale waves are observed in the winter stratosphere, and medium and synoptic-scale waves are limited to the troposphere and the UTLS (below ~20 km). Note that

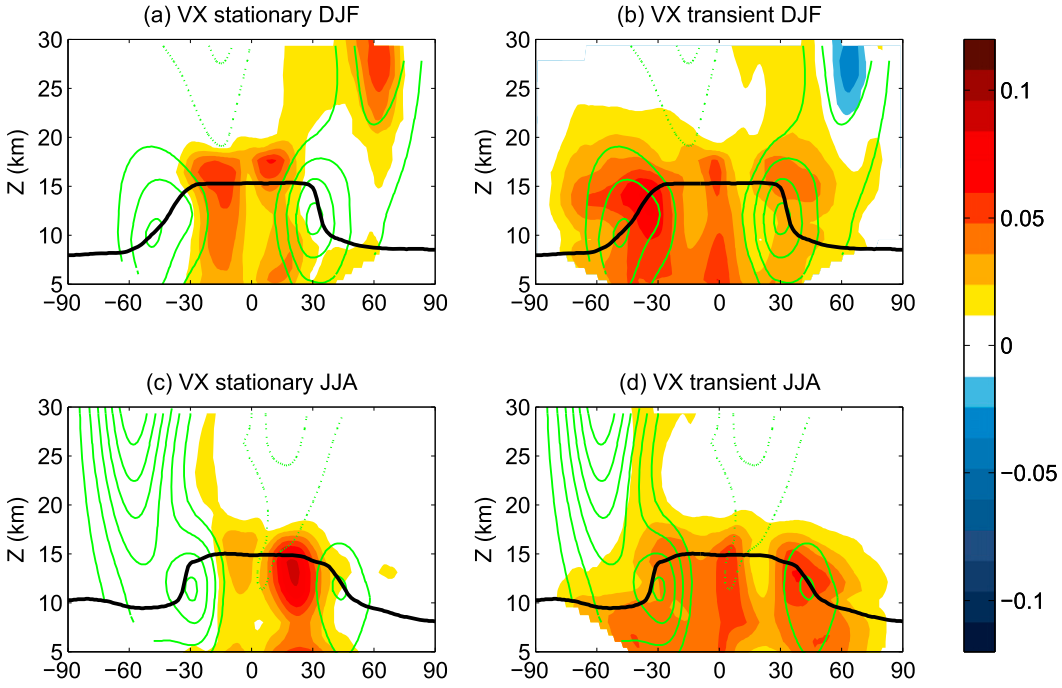

FIG. 4. Contributions to the eddy tracer flux ($\overline{v'_r\chi'}$; m s^{-1}) from (a),(c) stationary (monthly mean) and (b),(d) transient (all minus stationary) waves for (top) DJF and (bottom) JJA. The green contours show the zonal-mean wind with a 10 m s^{-1} spacing (solid for: positive, dotted for negative). The black contour shows the lapse-rate tropopause.

planetary-scale waves dominate the extratropical eddy flux in the summer UTLS poleward of the jet. While most planetary-scale eddies are stationary, these extratropical summer eddies are transient (cf. Figs. 5a,c to Figs. 4a,c). Figures 4 and 5 demonstrate that the large eddy tracer fluxes in the tropical UTLS are linked to stationary planetary-scale waves. This is consistent with previous results for dynamical eddies (Calvo and Garcia 2009). In particular, we find that wavenumber 1 dominates the strong eddy fluxes in this region for both seasons (not shown). As a note, while for planetary wavenumbers 1 and 2, positive stationary fluxes compensate the negative transient fluxes near the NH polar jet core (as seen in Fig. 4), for wavenumber 3 both stationary and transient fluxes are negative (not shown).

To further interpret the wave-driven tracer transport in the tropical UTLS we examine maps of the products of eddy quantities $v'_r\chi'$ before averaging zonally. Figures 6a and 6c show maps of the stationary eddy tracer product at 380 K for both seasons, together with the nondivergent circulation and the tracer structure. We choose this level because both the stationary and the transient eddies are large in both seasons, but the results are qualitatively similar for other levels in the UTLS. The stationary products are connected to the global tropical circulation, which closely resembles the idealized Gill–Matsuno response to deep convection (Gill 1980; Dima et al. 2005). In boreal winter (DJF; Fig. 6a) the main convective sources are located in the western Pacific, leading to two large anticyclones symmetric around the equator, which at this level extend across the Pacific Ocean [note that Dima et al. (2005) show the circulation at 150 hPa, which is ~5 km lower than the 380-K level shown in Fig. 6]. A smaller pair of quasi-symmetric anticyclones is observed over South America (centered around 80°W). These structures shape the equatorward flank of the subtropical jets, as shown by the wind vectors in Fig. 6, and the tracer structure closely follows the undulations of the subtropical jets (shown by the contours). Enhanced stationary eddy products are observed along the regions of strong undulations of the wind and tracer structure on the equatorward edge of the subtropical jets.

In boreal summer (JJA; Fig. 6c) the main source of convective heating is away from the equator at higher latitudes in the NH (over Southeast Asia). This results in different tropical circulation patterns, with a strong anticyclone on the NH centered around 25°N, 90°E (linked to the Asian summer monsoon) and a corresponding anticyclone in the southern tropics [at lower levels these are connected by a cross-equatorial circulation; see Dima et al. (2005)]. These circulation patterns are

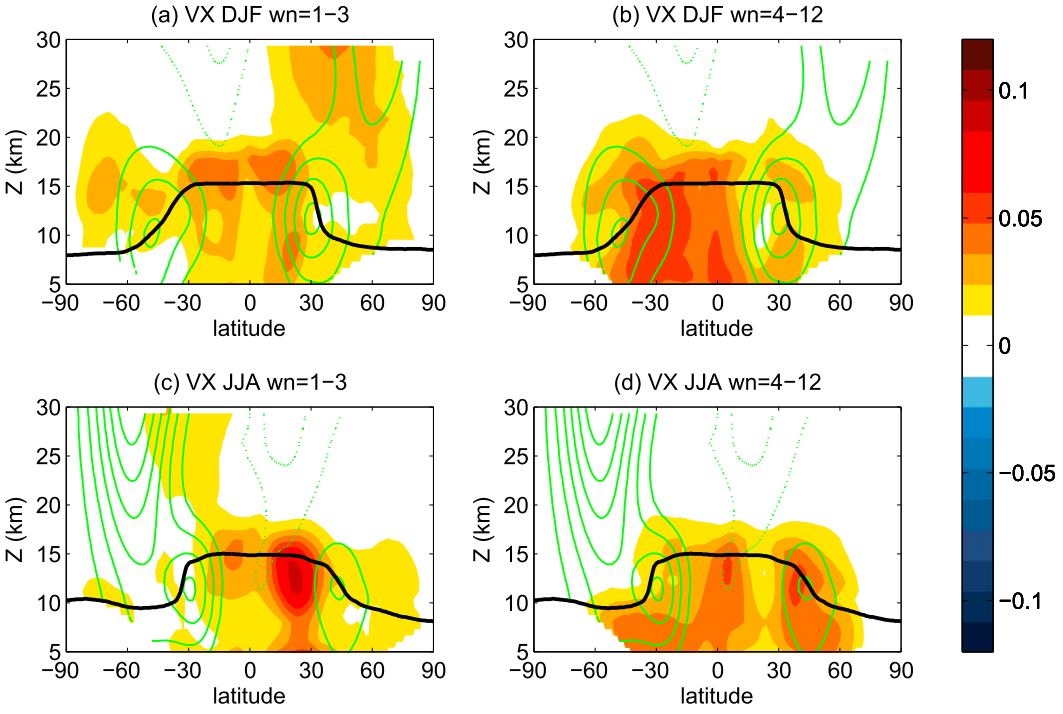

FIG. 5. Contributions to the eddy tracer flux ($\overline{v_r'\chi'}$; m s^{-1}) from (left) planetary-scale (wavenumbers 1–3) and (right) medium-scale (wavenumbers 4–7) waves for (top) DJF and (bottom) JJA. The green contours show the zonal-mean wind with a 10 m s^{-1} spacing (solid for positive, dotted for negative). The black contour shows the lapse-rate tropopause.

clearly seen in Fig. 6c both in the isentropic wind and the tracer concentrations. The resulting tracer eddies are closely coupled to the background circulation. There are strong opposite-sign eddy tracer products on the eastward and westward flanks of the Asian monsoon anticyclone, as well as a region of positive flux outside the eastern flank coinciding with a tongue of tracer transported from the extratropics into the tropics. While the strong centers inside the anticyclone largely cancel each other in the zonal mean, the maximum in Fig. 4c is linked to the stationary eddy product on the eastern side of the anticyclone. This in-mixing eddy transport process has been highlighted as an important transport mechanism for ozone concentrations near the tropical tropopause (Konopka et al. 2010; Abalos et al. 2013). There are also stationary tracer products associated with the corresponding anticyclone in the SH Indian Ocean.

The transient component of the eddy tracer products (Figs. 6b,d), computed as the total daily products minus the stationary products, is dominated by positive values. In both seasons the transient eddy products are found around the anticyclonic stationary structures described above. Equatorial transients are observed in DJF over regions of westerly winds, such as the central Pacific and east of South America. In JJA the strongest transient fluxes are found over the region of easterly winds south of the Asian monsoon anticyclone. These equatorial transients will be further explored in the next section. Overall, the eddies that drive isentropic tracer transport in the UTLS equatorward of the subtropical jets (see Fig. 2) are closely tied to the global tropical circulation linked to climatological deep convection.

Although not shown here, the eddy PV products have very similar patterns to the tropical eddy tracer products, both for the stationary and the transient waves. We note that in the UT, for instance at the level of 350 K, the PV eddy fluxes are comparatively small, as a result of the small PV gradients in this region. This constitutes a limitation of the PV as compared to the artificial tracer, which allows for identifying these features equally in any region given its uniform meridional gradient (at initialization). In addition, positive eddy products at 350 K are seen for the PV at the exits of storm tracks in the boreal winter jet and over the eastern portions of the Atlantic and Pacific basins in boreal summer, which result in the upgradient PV fluxes seen in Fig. 2d.

4. Phase-speed spectra

We examine the phase-speed spectra of the eddy tracer flux at different levels spanning the UTLS to

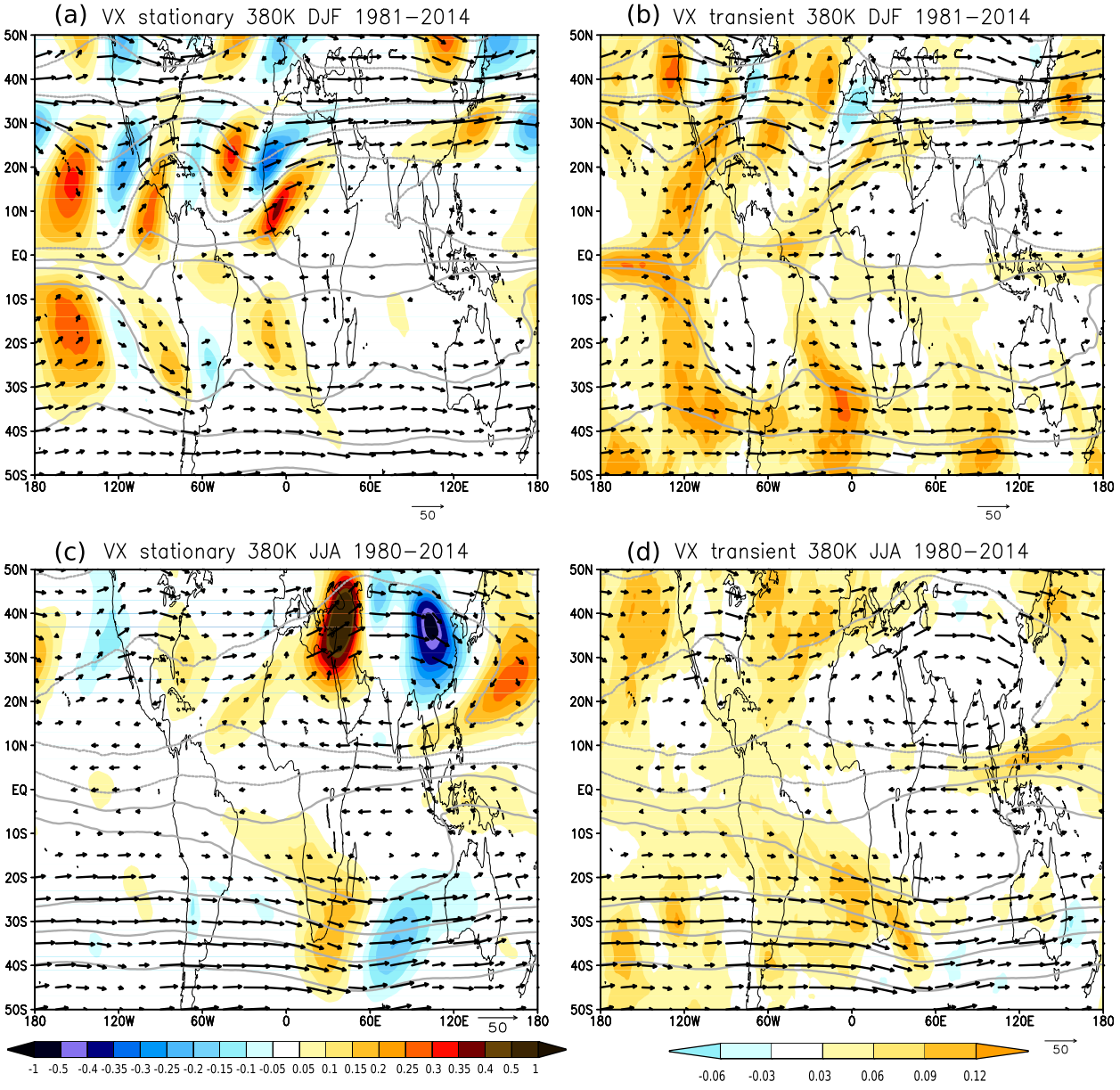

FIG. 6. Maps of the eddy tracer products ($v'_r\chi'$; color shading; m s^{-1}) at 380 K for (a),(c) stationary and (b),(d) transient waves in (top) DJF and (bottom) JJA. The arrows show the isentropic nondivergent wind climatology for each season, with the scale shown below each panel, and the meridional component is multiplied by 2 for better visualization. Vectors are plotted only when the magnitude of the total wind is larger than 5 m s^{-1}. Gray contours show the tracer climatology for each season, with 0.1 contour spacing (adimensional).

quantify the relationship of the eddy fluxes to the background zonal wind structure. We present separate spectra for the planetary-scale waves and the medium-scale waves, which we have defined as wavenumbers 1–3 and 4–7, respectively. Note that only transient eddy fluxes are represented in these space–time cospectra (Randel and Held 1991).

Figure 7 shows the cospectrum of $\overline{v'_r\chi'}$ at 320 K. This level has a steep latitudinal slope along the lower flank of the subtropical jets, connecting the extratropical lower stratosphere with the tropical lower troposphere (see Fig. 2). The spectra show that the phase speed of the tracer eddies is mainly westward with respect to the mean flow (consistent with Rossby waves), and the co-spectral density closely follows the shape of the background wind. Consistent with Fig. 5, there is a dominant role of medium-scale transients, with small power associated with planetary-scale waves, which are observed

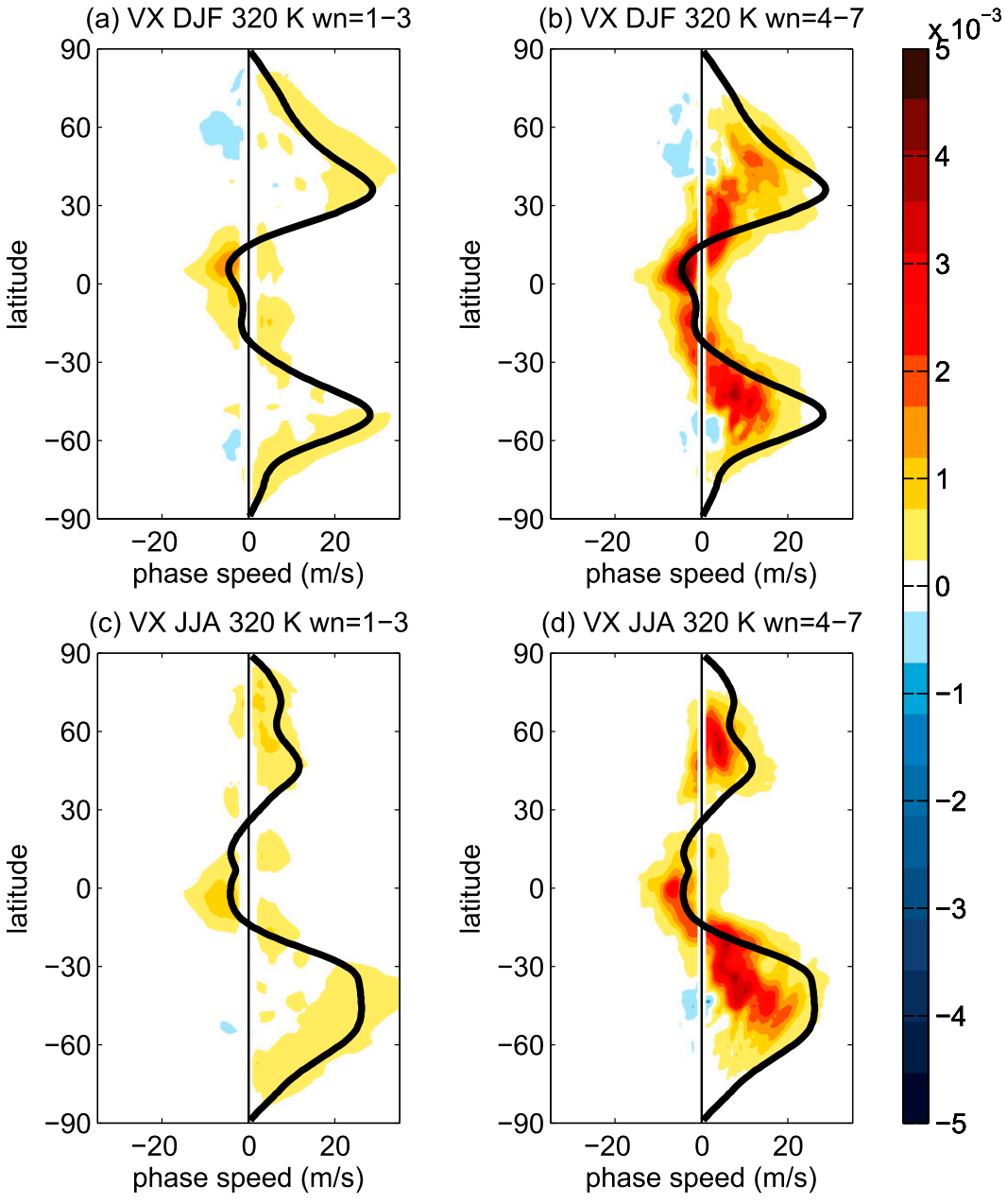

FIG. 7. Eddy tracer flux ($\overline{v'\chi'}$; m s^{-1}) cospectrum (color shading) at 320 K for (a),(b) DJF and (c),(d) JJA, separating (left) planetary-scale (wavenumbers 1–3) from (right) medium-scale waves (wavenumbers 4–7). The black line indicates the seasonal-mean zonal-mean wind at this level. The cospectrum is multiplied by the cosine of latitude.

mainly at high latitudes and in the deep tropics in both seasons. The predominance of the medium-scale waves in the transient eddy fluxes is partly due to the fact that most planetary-scale waves are quasi stationary (as seen in Figs. 4 and 5). In general, the medium-scale waves have phase speeds close to the background flow on both flanks of the jets, especially on the equatorward flank, in both seasons. Midlatitude medium-scale waves are especially close to their critical lines (where $c = \overline{u}$) in boreal summer, where the winds are weak, and thus waves are more likely to break and stir the tracer in this season.

Note that the phase speeds sometimes exceed the local climatological critical line. This behavior might be explained by the large variability in the zonal wind values on daily to interannual time scales (see section 5). When the entire range of variability in the wind is considered, the phase speeds of the eddy fluxes are

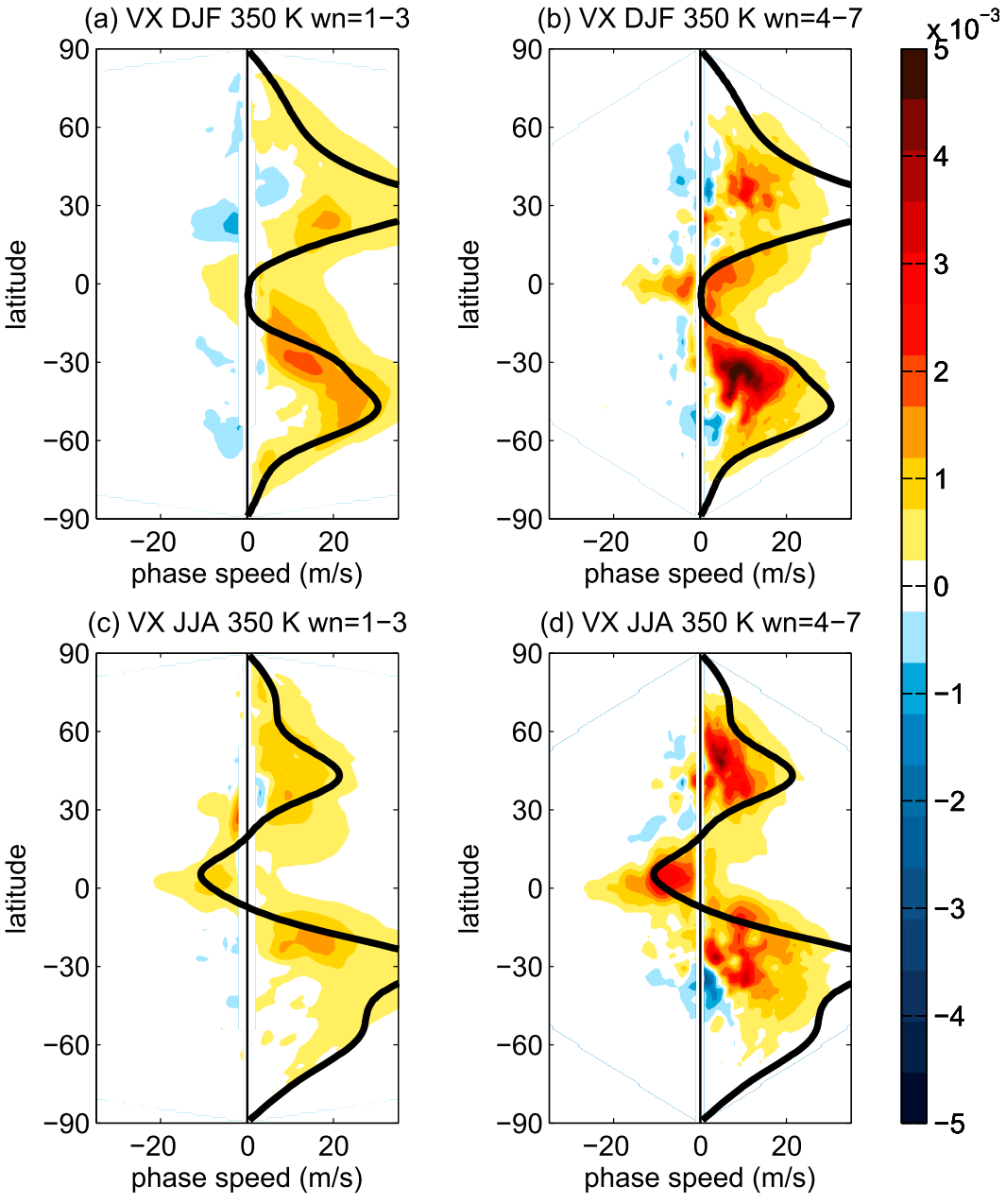

FIG. 8. As in Fig. 7, but at 350 K.

westward of the maximum wind speed values at every latitude and level (not shown).

The level of 350 K is representative of the tropical upper troposphere; it is almost parallel to a pressure surface (~200 hPa, ~12 km) and crosses both subtropical jets near their core. Figure 8 shows strong transient eddies at this level in both summer hemispheres, in the deep tropics, and on the equatorward side of the winter jet. The phase speeds of the eddy fluxes are again generally westward with respect to the background wind, consistent with the westward intrinsic phase speeds of Rossby waves. There is small eddy flux power at the core and on the poleward side of the winter jet, consistent with Figs. 2 and 4. Near the winter jet core, the phase speeds of the medium-scale waves are smaller than the speed of the background wind and thus far from the critical lines, consistent with lack of wave breaking and with the fact that the jet core acts as a waveguide and as a barrier for eddy transport. In middle latitudes the dominant phase speed of medium-scale

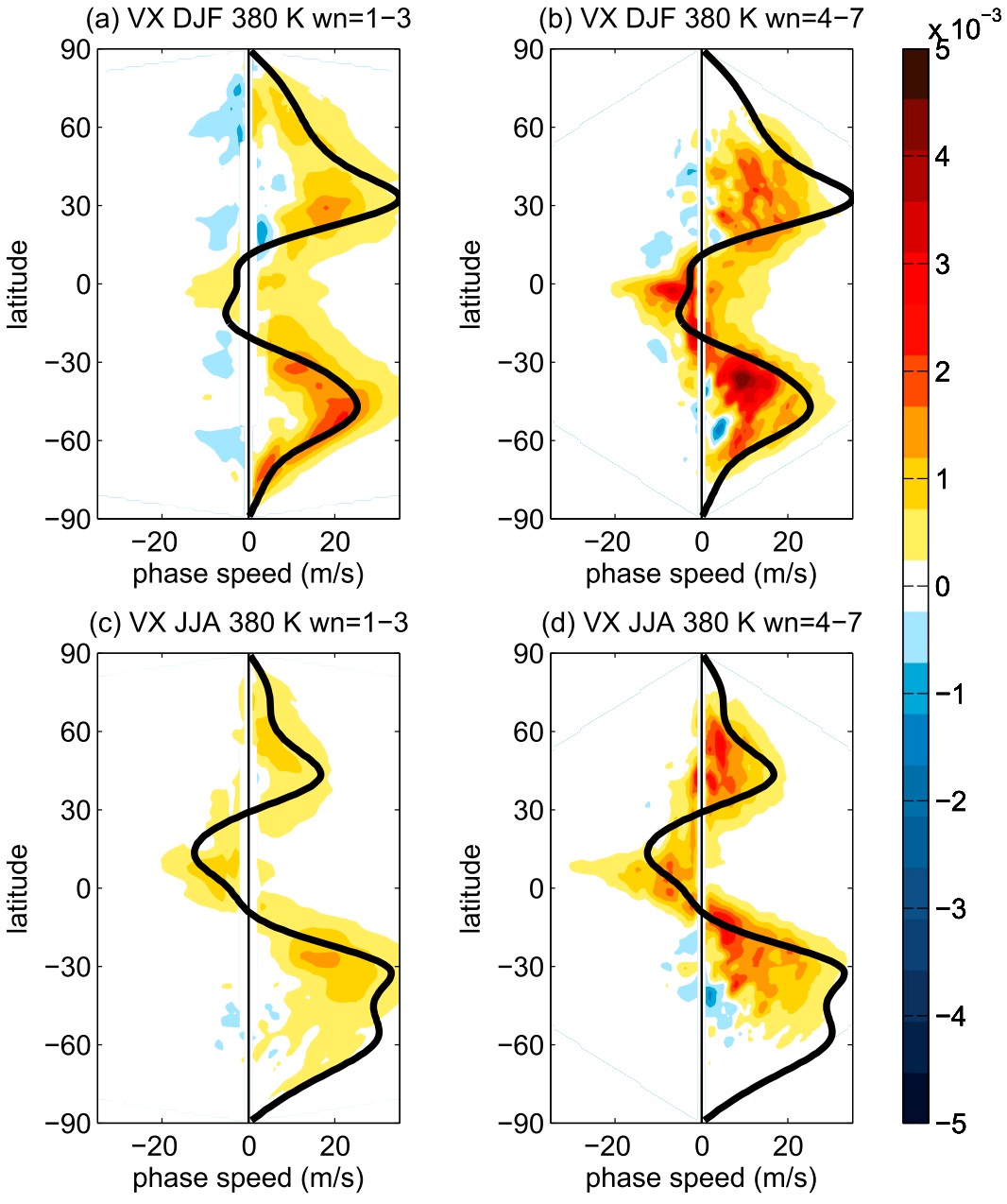

FIG. 9. As in Fig. 7, but at 380 K.

eddies is smaller than that of planetary eddies, with the latter closely following the critical lines. Overall, Fig. 8 shows that medium-scale transient Rossby waves are close to their critical lines in the summer hemisphere when the subtropical jet is weaker and on the equatorward flank of the jet in the winter hemisphere.

To analyze the region just above the subtropical jets, Fig. 9 shows the spectrum at 380 K. This level is characterized by strong stationary and transient eddy fluxes, with transients extending poleward of the jets, especially in the summer hemisphere (Fig. 4). Figure 9 is overall very similar to Fig. 8, except the transients at high latitudes (dominated by planetary-scale waves) extend farther poleward, especially in the summer hemisphere. This difference is seen most clearly in austral summer (SH in DJF), because in boreal summer (NH in JJA) the 350-K isentrope is slightly higher than the region of weakest fluxes poleward of the jet (which approximately follows the tropopause; see Fig. 2). In addition, the winds in the winter hemisphere on the upper flank of the

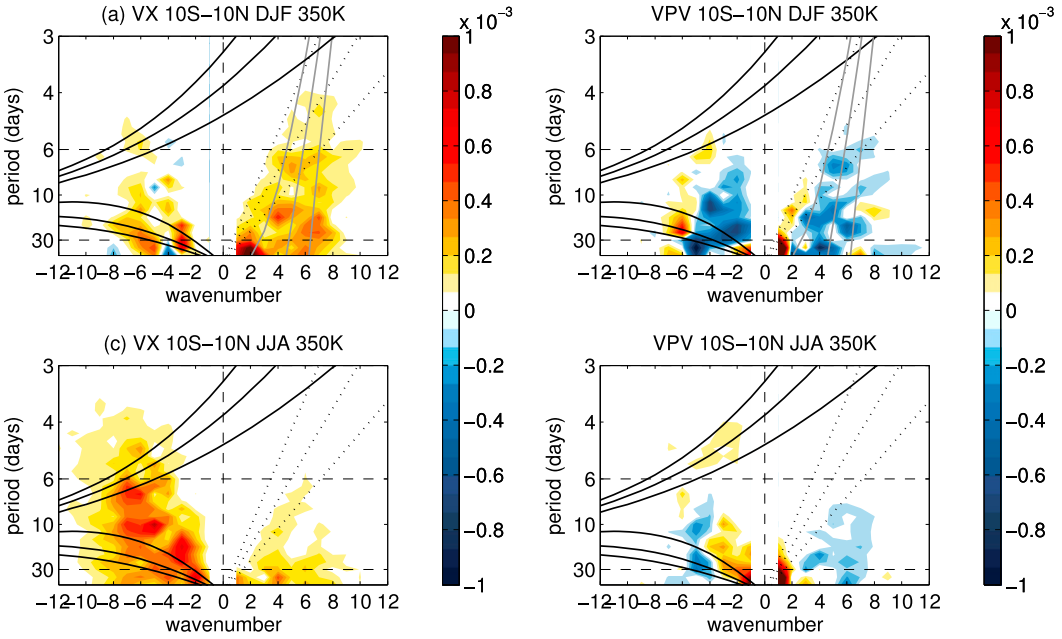

FIG. 10. Wavenumber–frequency (the latter expressed as period; days) representation of the near-equatorial (averaged over 10°S–10°N) (a),(c) eddy tracer flux ($\overline{v_r'\chi'}$; m s^{-1}) and (b),(d) eddy PV flux ($\overline{v'\mathrm{PV}'}$; PVU m s^{-1}) cospectrum (color shading) at 350 K for (top) DJF and (bottom) JJA. Solid black lines indicate theoretical equatorial dispersion relations for equatorial Rossby waves (westward), and mixed Rossby–gravity waves (westward and eastward). Kelvin wave dispersion lines are shown by the dotted lines. The dispersion lines for equatorial waves are the same shown in Wheeler and Kiladis (1999). The gray dispersion lines in (a) and (b) are extratropical Rossby waves computed from zonal wind at 30°N for meridional wavenumber $l = 1$, 5, and 7. Dashed lines show reference grid lines.

jet (380 K) are weaker than at the jet core (350 K), and thus the eddies are closer to their critical lines at the upper level. There are very small fluxes at high latitudes in the SH during JJA because the isentrope encounters the lowermost part of the polar jet, and these strong winds act as a barrier for eddy transport (see Fig. 2). The transient eddy fluxes in Fig. 9 [and more specifically their divergence; see Eq. (1)] are responsible for the strong stirring leading to the rapid tracer spread above the summer jets seen in Fig. 1.

Note that strong eddy tracer fluxes are observed close to the equator in Figs. 7–9 during both seasons (consistent with Figs. 4b and d). To investigate possible relationships with equatorial waves, Figs. 10a and 10c show the frequency–wavenumber decomposition of the eddy tracer flux near the equator at 350 K in DJF and JJA, following the methodology in Wheeler and Kiladis (1999). No background spectrum has been removed in Fig. 10, but the results are qualitatively the same when removing it (not shown). The results in Fig. 10 are representative of the layer ~320–380 K, although there are some variations with altitude. The equatorial eddy tracer fluxes at 350 K show a strong seasonal signature, with eastward-moving waves dominating in DJF and westward in JJA. At other levels above and below 350 K, the eastward DJF fluxes are weaker, and the flux is mostly westward in both seasons, especially in the lower troposphere (not shown). The westward fluxes, dominant in JJA but also present in DJF, have a spectral signature similar to westward-traveling equatorial Rossby waves (ERW), with periods between 6 and 30 days and wavenumbers between 2 and 8. Maps for individual events of strong flux highlight tracer concentrations from the subtropics wrapped around the traveling Rossby anticyclones on both sides of the equator, with filaments frequently crossing the equator (not shown). In JJA, the strongest transient eddy fluxes associated with westward-propagating waves are found southeast of the Asian monsoon anticyclone (see Fig. 6d).

Figures 10b and 10d show the corresponding spectra for the eddy PV flux, highlighting important similarities with the tracer flux. In particular, the similarity of the two spectra in DJF suggests that the eastward power cannot be attributed to Kelvin waves, as these waves have no PV signature (Gill 1982). Note that this is not evident because, although Kelvin waves have $v' = 0$, the rotational part of the wind has a spurious Kelvin wave signature ($v_r' \neq 0$), which could be transferred to the tracer eddy flux. Instead, we suggest that the power on

this side of the spectrum is mainly linked to Rossby waves of extratropical origin (periods longer than 6 days and wavenumbers between 2 and 8), propagating over regions of equatorial westerly winds. The regions of equatorial westerlies where these Rossby waves can propagate are often referred to as westerly ducts (Webster and Holton 1982; Waugh and Polvani 2000; Hitchman and Huesmann 2007; Barnes and Hartmann 2012; Albers et al. 2016) and occur preferentially in boreal winter over the Pacific and Atlantic Oceans. The spatial distribution of the transient eddy products seen in Fig. 6b is indeed concentrated over the westerly ducts in DJF. Moreover, this signal maximizes at 350 K, consistent with the characteristics of the westerly ducts. The dispersion curves for these extratropical waves are shown in Fig. 10, and they capture the power on this side of the spectrum better than the Kelvin wave dispersion lines. The curves have been derived using the simplified dispersion relation for barotropic Rossby waves at 30°N, $\omega = k\overline{u} - k\beta_{\text{eff}}/(k^2 + l^2)$, with $\beta_{\text{eff}} = \beta - u_{yy}$, which capture the eastward power spectrum of v_r' at 30°N (not shown). The relevance of the extratropical waves and the westerly ducts in the equatorial upper troposphere is not seen in previous studies of equatorial frequency–wavenumber analyses (Kiladis et al. 2009). This is because it becomes evident when isolating the rotational component of the flow and is not present in temperature or outgoing longwave radiation (not shown).

There is an additional strong eastward component peaking at low wavenumbers (1–2) and periods longer than 30 days in DJF. This low-frequency signal is observed throughout the tropical upper troposphere (up to 380 K), and it is likely associated with the rotational flow component of the Madden–Julian oscillation (MJO). This signature is not seen in the PV flux. The positive values in the PV flux correspond to the equatorial positive fluxes seen in Fig. 2, which are linked to generation of quasi-stationary waves coupled to convection. Finally, note that the PV flux westward component in JJA is much weaker, consistent with a smaller signal of inmixing around the Asian monsoon anticyclone in PV as compared to the passive tracer (not shown). We highlight again that our analyses, based on the rotational component of the flow, neglect the divergent component of the total wind field, which is not negligible in the tropical UTLS. Hence, while this configuration allows the interesting features for transient eddies discussed above to arise, it restricts our ability to extract general conclusions regarding cross-equatorial tracer transport, as discussed in section 6.

Figure 11 shows the phase-speed spectrum at 450 K, a level located in the lower stratosphere (see Fig. 2). There is a substantial change between the 380-K level and the 450-K level, with much weaker fluxes at the upper level. This is mainly due to reduced flux linked to smaller-scale eddies, which are dissipated at lower levels (the planetary-scale eddies are relatively less reduced). In DJF there are planetary and medium-scale eddies with phase speeds very close to the weak background winds in both hemispheres, which means they are close to dissipating. As in other levels, at high latitudes only planetary-scale eddies are found. In JJA there are strong winds at high latitudes in the SH, linked to the lower part of the SH polar night jet, and both planetary and medium-scale eddies are confined to the equatorward edge of the vortex.

In the middle stratosphere (e.g., 650 K, not shown), the surf zone is highlighted as a region of strong planetary transient eddy flux, which adds to the stationary flux (see Fig. 4). Negative planetary-scale transient eddy fluxes are found at the core of the NH polar vortex, linked to wave formation during wave breaking processes as discussed above. These negative transients are characterized mainly by planetary-scale wavenumbers and small phase speeds (between +5 and $-5\,\text{m}\,\text{s}^{-1}$). In the summer hemisphere there is a smaller but nonzero (positive) eddy flux associated with westward-traveling waves, as described by Wagner and Bowman (2000).

Overall, medium-scale eddies dominate the spectra especially in the subtropical and midlatitude UTLS, while the weaker planetary eddy fluxes dominate at high latitudes. Note that this distribution can be attributed at least partly to the spherical geometry, since for a constant Rossby radius of deformation the wavenumber decreases with latitude. In the UTLS, the eddies are close to the critical lines in the summer hemisphere and on the equatorward flank of the jet in the winter hemisphere. The relative importance of planetary- versus medium-scale transient eddy fluxes increases with altitude. The phase speeds of the eddies are westward with respect to the background zonal wind, with some spread linked to variability in the wind (see section 5). These results are in agreement with previous studies of transport by Rossby wave breaking (e.g., Hitchman and Huesmann 2007; Homeyer and Bowman 2013; Barnes and Hartmann 2012).

5. Interannual variability

Although an extensive analysis of interannual variability in eddy transport is beyond the scope of this paper, in this section we briefly explore the influence of El Niño–Southern Oscillation (ENSO) and the quasi-biennial oscillation (QBO) on the eddy tracer

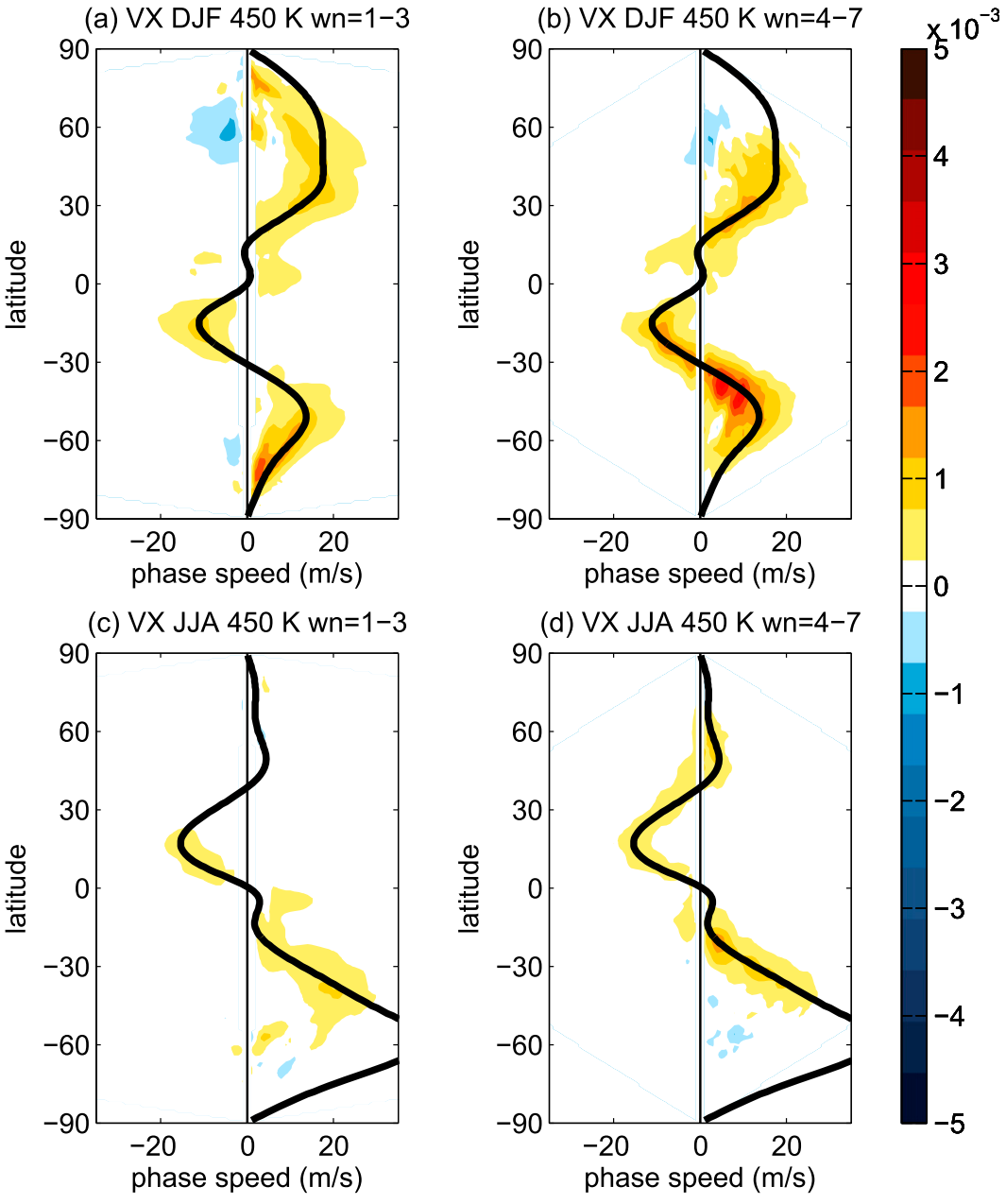

FIG. 11. As in Fig. 7, but at 450 K.

fluxes. These sources of variability account for part of the spread in the eddy tracer fluxes around the climatological critical lines (in addition to day-to-day variability).

Figures 12a and 12b show composites of the (total) eddy tracer flux for the positive-minus-negative phases of ENSO and QBO in DJF (qualitatively similar results are found for JJA, not shown). The index chosen for ENSO is the multivariate ENSO index (Wolter and Timlin 1998), and the index chosen for the QBO is the second empirical orthogonal function (EOF) of the zonal-mean wind between 70 and 10 hPa at the equator (which captures most of the wind variance in the tropical lower stratosphere) (Wallace et al. 1993). The positive and negative cases are defined as deviations larger than one standard deviation from the climatological average for each season. The changes in eddy fluxes in Fig. 12 are consistent with the composites of the effective diffusivity shown in Abalos et al. (2016). The positive phase of ENSO [El Niño (EN)] strengthens the equatorward

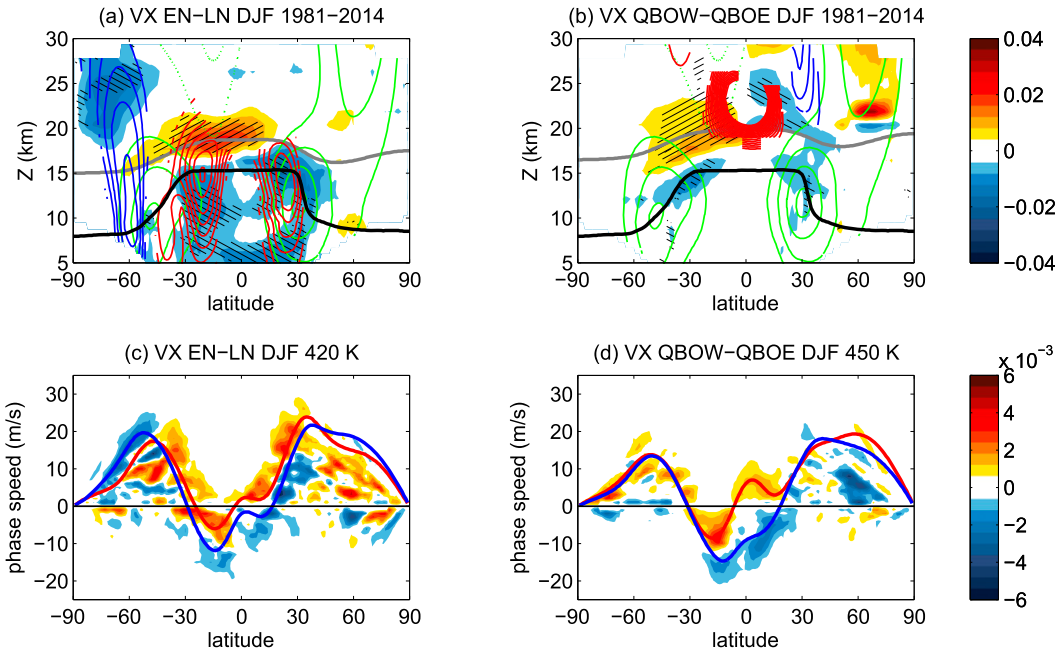

FIG. 12. (a) EN minus LN (EN − LN) and (b) QBO-west minus QBO-east (QBOW − QBOE) composites of eddy flux (color shading) and zonal wind (contours; red for positive, blue for negative) for DJF. The green contours are the zonal-mean-wind climatology. The black line indicates the tropopause. The gray line shows the 420 (450)-K isentropic level in the ENSO (QBO) panel. Hatching indicates the regions of statistical significance at the 95% confidence level using the Student's t test. (bottom) Difference of eddy tracer flux cospectrum (shading) for (c) EN − LN cases at 420 K and (d) QBOW − QBOE cases at 450 K in DJF. The red (blue) solid contours show the mean-wind line during EN and QBOW (LN and QBOE) phases. The cospectrum is multiplied by the cosine of latitude.

flank of the subtropical jets, and the eddy flux is reduced in the tropical upper troposphere (Fig. 12a). The negative wind contours in the SH in DJF reflect the strengthened southern annular mode (SAM) during the negative ENSO phase [La Niña (LN); e.g., Chen and Held 2007], which results in enhanced wave propagation and eddy flux during this phase (leading to negative values between 20 and 30 km in Fig. 12a). Above the subtropical jet there is a region of positive tracer flux anomalies. This is consistent with the westerly zonal wind anomalies in this region of climatological near-zero winds. Corresponding positive anomalies were also found in effective diffusivity in Abalos et al. (2016). The QBO composite (Fig. 12b) shows enhanced eddy flux in the summer side of the equatorial zonal wind anomalies, similar to the QBO anomalies in effective diffusivity shown in Abalos et al. (2016) (although in that paper the results for the first EOF are presented, which peaks in the middle stratosphere). The mechanism for this behavior, as explained by Shuckburgh et al. (2001), is that westerly winds during the QBO-west (QBOW) phase lead to increased cross-equatorial eddy transport from the winter into the summer hemisphere.

Figures 12c and 12d show the corresponding anomalies in the phase-speed spectra at 420 K for the ENSO composite and 450 K for the QBO composite; these levels are located in the region of positive anomalies in the lower stratosphere, as shown in Figs. 12a and 12b. Note that the composites in Figs. 12a and 12b result from the sum over all phase speeds of the cospectrum, plus the contribution from the stationary waves. The zonal wind is shown for the positive and the negative phases. In both cases, positive (negative) anomalies in the cospectrum closely follow the critical line corresponding to the positive (negative) phase of the indices, indicating a shift in the phase speeds of the eddy fluxes associated with the shift in the background wind. For ENSO (Fig. 12c), positive anomalies are observed throughout the subtropics equatorward of the maximum zonal wind (around 40°N/S). Near cancellation of positive and negative anomalies for different phase speeds occurs in the NH subtropics, implying a change in the phase speeds of the eddies during different ENSO phases. In contrast, in the SH subtropics mainly positive anomalies are seen (leading to stronger positive anomalies in the summer hemisphere net eddy flux; Fig. 12a), implying that the eddy fluxes in this region are only present (or at

least strengthened) during the EN phase. Negative values are observed in high latitudes, linked to the stronger SAM during the LN phase as discussed above. The QBO composite (Fig. 12d) shows a clear shift in the eddy fluxes' phase speeds in the tropical region between easterly and westerly phases. Note that adding up the anomalies for all phase speeds gives negative net eddy flux in the winter tropics and positive in the summer tropics (consistent with Fig. 12b). In summary, ENSO and the QBO can have an impact on the eddy tracer fluxes by changing the location of their critical lines above the subtropical jets.

6. Summary and discussion

We have examined the spectral characteristics of the waves leading to large-scale stirring and mixing in the UTLS using an artificial passive tracer. The tracer is conserved on each isentrope individually, it is advected by the ERA-Interim two-dimensional (nondivergent) isentropic flow, and it is subject to small-scale diffusion. The evolution of the tracer highlights the inhomogeneity of the mixing strength at different levels and latitudes (Fig. 1), consistent with the spatial patterns of effective diffusivity shown in previous studies (Haynes and Shuckburgh 2000a,b; Allen and Nakamura 2001; Abalos et al. 2016). The focus of this work is to quantify the associated eddy tracer fluxes and evaluate their space–time spectral behavior.

It is important to stress that, as in previous works, the transport on isentropes is assumed to follow simple 2D barotropic dynamics, with $\nabla \cdot \mathbf{u} = 0$ and the tracer continuity equation [Eq. (1)]. However, we note that an equally valid alternative is to define the nondivergent flow on isentropes as satisfying $\nabla \cdot (\sigma \mathbf{u}) = 0$, in which case the tracer equation is [equivalent to Eq. (9.4.21) in Andrews et al. (1987)]

$$\overline{\chi}_t^* = -\overline{\sigma}^{-1}(\overline{\hat{v}_r \sigma \hat{\chi}})_y + \overline{S}^*, \tag{4}$$

where $\overline{A}^* = \overline{\sigma A}/\overline{\sigma}$, $\hat{A} = A - \overline{A}^*$, and $\sigma = -g^{-1}p_\theta$ is the density on isentropes. In this case the inhomogeneity of the density on isentropes is taken into account. To what extent this might result in different eddy fluxes ($\overline{\hat{v}_r \sigma \hat{\chi}}$ vs $\overline{v_r' \chi'}$) remains to be studied.

The eddy tracer flux results show that stationary waves play an important role for tracer transport in the tropical UTLS, with significant stationary eddy tracer transport linked to the Asian monsoon anticyclone in JJA (Figs. 4,6). Large stationary fluxes are also found in the winter stratosphere, together with planetary-scale transients (Fig. 4). Transient eddies are observed around the upper and lower flanks of the subtropical jets, extending poleward into the extratropics especially in the summer lower stratosphere (Fig. 4). The isentropes crossing the subtropical jets are characterized by weak eddy fluxes and small tracer transport at the jet core and poleward of it, especially in the winter hemisphere (Fig. 2). While in general medium-scale waves (wavenumbers 4–7) dominate the transient eddy fluxes, planetary transient waves are most important at high latitudes (cf. Figs. 4 and 5).

The phase-speed spectra (Figs. 7–11) at different levels across the UTLS show eddy tracer fluxes with phase speeds westward relative to the background zonal wind (consistent with Rossby waves), and in general closely following the critical lines. This behavior has been shown in previous works for dynamical eddy fluxes (Randel and Held 1991), highlighting that the linear theory of wave propagation can be used to understand observed characteristics of wave–mean flow interaction. In the present work it is first shown that the eddy tracer fluxes are closely related to the mixing properties in the UTLS (Fig. 3). Then the analysis of the phase-speed spectra demonstrates that the critical lines arise as fundamental properties of the flow strongly influencing eddy tracer transport and mixing. Figures 7–11 show that medium-scale waves (wavenumbers 4–7) dominate the transient eddy fluxes around the subtropical jets in the UTLS. In the middle stratosphere (not shown) planetary-scale transient eddies in the surf zone largely dominate the spectra, and negative transient tracer fluxes near the jet core in the NH winter are linked to wave generation (see Fig. 4).

Near-equatorial transient eddy fluxes are found throughout the upper troposphere (e.g., Figs. 8, 9). These are mainly linked to westward-moving waves associated with the Asian monsoon anticyclone in boreal summer and to (eastward) Rossby waves of extratropical origin in boreal winter (Fig. 10), which cross the equator over the westerly ducts in the Pacific and Atlantic Oceans (Waugh and Polvani 2000). We have estimated the interhemispheric turnover time scales associated with this cross-equatorial Rossby wave transport by dividing the flux at the equator by the hemispherically averaged tracer concentration. The results give time scales of about one year at altitudes in the UTLS, which is not negligible compared to the radiative time scales near the tropical tropopause. There is a steep vertical structure, with turnover time scales an order of magnitude longer in the stratosphere, consistent with steeper tracer meridional gradients in the tropical stratosphere (see Fig. 1). However, we highlight that our analyses provide information exclusively on the two-dimensional nondivergent isentropic component of transport. While this is in general a good approximation in middle latitudes, in the tropical upper troposphere the

divergent flow is not negligible (for instance, the Hadley circulation is not included in these analyses). This implies that the net three-dimensional eddy tracer fluxes in this region can differ substantially from those considered here. In particular, the Hadley circulation likely makes an important contribution to the net hemispheric turnover time scale. Additional work beyond the scope of this paper is needed to evaluate the contribution of the rotational component to the net interhemispheric transport. On the other hand, the specific configuration of our analyses allows examination of the spectral characteristics of the rotational flow alone. Space–time spectral analyses in the tropics are usually focused on variables linked to the divergent flow and proxies for convection (e.g., Wheeler and Kiladis 1999; Kiladis et al. 2009). Our artificial tracer setting, initially designed to examine the extratropical circulation, provides an opportunity to investigate the rotational component of the tropical circulation, and the results reveal interesting features.

The analysis of the eddy transport fluxes can be done alternatively using potential vorticity as a quasi-conserved tracer on isentropes. The PV eddy flux results are highly consistent with the artificial passive tracer, and the eddy diffusivity is qualitatively similar to that in Fig. 3 (not shown). This is consistent with the good agreement found in Abalos et al. (2016) between the effective diffusivity calculations based on the artificial tracer and on PV. The wave decomposition of the flux is overall consistent as well (not shown). The advantages of using the artificial tracer versus PV are twofold. First, it ensures tracer conservation and a simple balance between the tendency and the eddy transport term in the tracer continuity equation [Eq. (1)]. This is particularly important in regions where PV has strong diabatic sources, such as the summer subtropics and the equatorial upper troposphere (Fig. 2). Second, the artificial tracer is initialized at the beginning of each season with uniform meridional gradients such that eddy tracer fluxes in different regions are independent of initial gradients. Consequently, the seasonal-mean structure of artificial tracer concentrations shown in Fig. 1 results exclusively from the stirring and mixing processes (unlike PV). Another valid possibility is to use real tracers (Allen and Nakamura 2001; Gille et al. 2014; Abalos et al. 2016), although these are obviously not conserved on isentropes but are subject to diabatic transport and chemical sources and sinks, and the observations are limited. We have computed eddy diffusivity from ERA-Interim ozone, and the results are less consistent than those using PV, especially in the stratosphere, where the ozone chemistry plays an important role (not shown).

Finally, we have briefly analyzed the interannual variability of the eddy fluxes. The modulations in the zonal wind related to ENSO and the QBO modify the wave propagation conditions, and consistent behavior is observed for the phase speeds of the eddy tracer fluxes (Fig. 12). This demonstrates the dynamical mechanisms underlying the interannual variations in effective diffusivity recently analyzed in Abalos et al. (2016). This behavior further illustrates the strong control of the eddy tracer fluxes by the critical lines. For instance, future changes in the position of the critical lines predicted by climate models (Shepherd and McLandress 2011) can affect isentropic eddy transport in the upper flanks of the subtropical jets and thus tracer exchange between the tropics and extratropics and between the troposphere and the stratosphere. This can lead to changes in the distribution of chemical constituents in the UTLS, which in turn have an impact on surface radiative forcing (e.g., Riese et al. 2012). Understanding these interactions in detail involves quantifying the changes in the critical lines driven by the dynamical eddies (e.g., Barnes and Thompson 2014).

Acknowledgments. We are thankful to the reviewers for very insightful and constructive comments, which have substantially improved the paper. We thank G. Kiladis, J. Dias, J. Albers, and P. Hitchcock for discussions and R. Garcia for comments on an earlier version of the manuscript. M. Abalos was supported by a grant of the NASA ACMAP program (NNX15AE48G). T. Birner acknowledges funding from the Climate and Large-Scale Dynamics Program of the National Science Foundation (1151768). ERA-Interim data were provided by the ECMWF. The data from this study are available from the authors upon request.

REFERENCES

Abalos, M., W. J. Randel, D. E. Kinnison, and E. Serrano, 2013: Quantifying tracer transport in the tropical lower stratosphere using WACCM. *Atmos. Chem. Phys.*, **13**, 10 591–10 607, doi:10.5194/acp-13-10591-2013.

——, B. Legras, and E. Shuckburgh, 2016: Interannual variability in effective diffusivity in the upper troposphere/lower stratosphere from reanalysis data. *Quart. J. Roy. Meteor. Soc.*, **142**, 1847–1861, doi:10.1002/qj.2779.

Albers, J. R., G. N. Kiladis, T. Birner, and J. Dias, 2016: Tropical upper-tropospheric potential vorticity intrusions during sudden stratospheric warmings. *J. Atmos. Sci.*, **73**, 2361–2384, doi:10.1175/JAS-D-15-0238.1.

Allen, D. R., and N. Nakamura, 2001: A seasonal climatology of effective diffusivity in the stratosphere. *J. Geophys. Res.*, **106**, 7917–7935, doi:10.1029/2000JD900717.

Andrews, D. G., J. R. Holton, and C. B. Leovy, 1987: *Middle Atmosphere Dynamics*. International Geophysics Series, Vol. 40, Academic Press, 489 pp.

Barnes, E. A., and D. L. Hartmann, 2012: Detection of Rossby wave breaking and its response to shifts of the midlatitude jet with climate change. *J. Geophys. Res.*, **117**, D09117, doi:10.1029/2012JD017469.

——, and D. W. J. Thompson, 2014: Comparing the roles of barotropic versus baroclinic feedbacks in the atmosphere's response to mechanical forcing. *J. Atmos. Sci.*, **71**, 177–194, doi:10.1175/JAS-D-13-070.1.

Birner, T., D. W. J. Thompson, and T. G. Shepherd, 2013: Up-gradient eddy fluxes of potential vorticity near the subtropical jet. *Geophys. Res. Lett.*, **40**, 5988–5993, doi:10.1002/2013GL057728.

Bönisch, H., A. Engel, J. Curtius, T. Birner, and P. Hoor, 2009: Quantifying transport into the lowermost stratosphere using simultaneous in-situ measurements of SF_6 and CO_2. *Atmos. Chem. Phys.*, **9**, 5905–5919, doi:10.5194/acp-9-5905-2009.

Bowman, K. P., and G. D. Carrie, 2002: The mean-meridional transport circulation of the troposphere in an idealized GCM. *J. Atmos. Sci.*, **59**, 1502–1514, doi:10.1175/1520-0469(2002)059<1502:TMMTCO>2.0.CO;2.

Calvo, N., and R. R. Garcia, 2009: Wave forcing of the tropical upwelling in the lower stratosphere under increasing concentrations of greenhouse gases. *J. Atmos. Sci.*, **66**, 3184–3196, doi:10.1175/2009JAS3085.1.

Charney, J. G., and P. G. I. Drazin, 1961: Propagation of planetary-scale disturbances from the lower into the upper atmosphere. *J. Geophys. Res.*, **66**, 83–109, doi:10.1029/JZ066i001p00083.

Chen, G., and I. Held, 2007: Phase speed spectra and the recent poleward shift of Southern Hemisphere surface westerlies. *Geophys. Res. Lett.*, **34**, L21805, doi:10.1029/2007GL031200.

——, and A. Plumb, 2014: Effective isentropic diffusivity of tropospheric transport. *J. Atmos. Sci.*, **71**, 3499–3520, doi:10.1175/JAS-D-13-0333.1.

——, J. Lu, and D. M. W. Frierson, 2008: Phase speed spectra and the latitude of surface westerlies: Interannual variability and global warming trend. *J. Climate*, **21**, 5942–5959, doi:10.1175/2008JCLI2306.1.

Dee, D., and Coauthors, 2011: The ERA-Interim reanalysis: Configuration and performance of the data assimilation system. *Quart. J. Roy. Meteor. Soc.*, **137**, 553–597, doi:10.1002/qj.828.

Dima, I. M., J. M. Wallace, and I. Kraucunas, 2005: Tropical zonal momentum balance in the NCEP reanalyses. *J. Atmos. Sci.*, **62**, 2499–2513, doi:10.1175/JAS3486.1.

Garcia, R. R., 1991: Parameterization of planetary wave breaking in the middle atmosphere. *J. Atmos. Sci.*, **48**, 1405–1419, doi:10.1175/1520-0469(1991)048<1405:POPWBI>2.0.CO;2.

Gill, A. E., 1980: Some simple solutions for heat-induced tropical circulation. *Quart. J. Roy. Meteor. Soc.*, **106**, 447–462, doi:10.1002/qj.49710644905.

——, 1982: *Atmosphere–Ocean Dynamics*. International Geophysics Series, Vol. 30, Academic Press, 662 pp.

Gille, J., S. Karol, D. Kinnison, J.-F. Lamarque, and V. Yudin, 2014: The role of midlatitude mixing barriers in creating the annual variation of total ozone in high northern latitudes. *J. Geophys. Res. Atmos.*, **119**, 9578–9595, doi:10.1002/2013JD021416.

Haynes, P., and E. Shuckburgh, 2000a: Effective diffusivity as a diagnostic of atmospheric transport: 1. Stratosphere. *J. Geophys. Res.*, **105**, 22 777–22 794, doi:10.1029/2000JD900093.

——, and ——, 2000b: Effective diffusivity as a diagnostic of atmospheric transport: 2. Troposphere and lower stratosphere. *J. Geophys. Res.*, **105**, 22 795–22 810, doi:10.1029/2000JD900092.

Hegglin, M. I., and T. G. Shepherd, 2007: O_3–N_2O correlations from the Atmospheric Chemistry Experiment: Revisiting a diagnostic of transport and chemistry in the stratosphere. *J. Geophys. Res.*, **112**, D19301, doi:10.1029/2006JD008281.

Hitchman, M. H., and A. S. Huesmann, 2007: A seasonal climatology of Rossby wave breaking in the 320–2000-K layer. *J. Atmos. Sci.*, **64**, 1922–1940, doi:10.1175/JAS3927.1.

Homeyer, C. R., and K. P. Bowman, 2013: Rossby wave breaking and transport between the tropics and extratropics above the subtropical jet. *J. Atmos. Sci.*, **70**, 607–626, doi:10.1175/JAS-D-12-0198.1.

Hoskins, B. J., M. E. McIntyre, and W. Robertson, 1985: On the use and significance of isentropic potential vorticity maps. *Quart. J. Roy. Meteor. Soc.*, **111**, 877–946, doi:10.1002/qj.49711147002.

Kiladis, G. N., M. C. Wheeler, P. T. Haertel, K. H. Straub, and P. E. Roundy, 2009: Convectively coupled equatorial waves. *Rev. Geophys.*, **47**, RG2003, doi:10.1029/2008RG000266.

Kim, H., and S. Lee, 2004: The wave–zonal mean flow interaction in the Southern Hemisphere. *J. Atmos. Sci.*, **61**, 1055–1067, doi:10.1175/1520-0469(2004)061<1055:TWMFII>2.0.CO;2.

Konopka, P., J.-U. Grooß, G. Günther, F. Ploeger, R. Pommrich, R. Müller, and N. Livesey, 2010: Annual cycle of ozone at and above the tropical tropopause: Observations versus simulations with the Chemical Lagrangian Model of the Stratosphere (CLaMS). *Atmos. Chem. Phys.*, **10**, 121–132, doi:10.5194/acp-10-121-2010.

Matsuno, T., 1970: Vertical propagation of stationary planetary waves in the winter Northern Hemisphere. *J. Atmos. Sci.*, **27**, 871–883, doi:10.1175/1520-0469(1970)027<0871:VPOSPW>2.0.CO;2.

McIntyre, M. E., and T. N. Palmer, 1983: Breaking planetary waves in the stratosphere. *Nature*, **305**, 593–599, doi:10.1038/305593a0.

Nakamura, N., 2008: Quantifying inhomogeneous, instantaneous, irreversible transport using passive tracer field as a coordinate. *Transport and Mixing in Geophysical Flows*, J. B. Weiss and A. Provenzale, Eds., Lecture Notes in Physics, Vol. 744, Springer, 137–164, doi:10.1007/978-3-540-75215-8_7.

Ploeger, F., and Coauthors, 2013: Horizontal water vapor transport in the lower stratosphere from subtropics to high latitudes during boreal summer. *J. Geophys. Res. Atmos.*, **118**, 8111–8127, doi:10.1002/jgrd.50636.

Plumb, R. A., 1996: A ''tropical pipe'' model of stratospheric transport. *J. Geophys. Res.*, **101**, 3957–3972, doi:10.1029/95JD03002.

——, and J. D. Mahlman, 1987: The zonally averaged transport characteristics of the GFDL general circulation/transport model. *J. Atmos. Sci.*, **44**, 298–327, doi:10.1175/1520-0469(1987)044<0298:TZATCO>2.0.CO;2.

Randel, W. J., and I. Held, 1991: Phase speed spectra of transient eddy fluxes and critical layer absorption. *J. Atmos. Sci.*, **48**, 688–697, doi:10.1175/1520-0469(1991)048<0688:PSSOTE>2.0.CO;2.

——, R. R. Garcia, and F. Wu, 2008: Dynamical balances and tropical stratospheric upwelling. *J. Atmos. Sci.*, **65**, 3584–3595, doi:10.1175/2008JAS2756.1.

Riese, M., F. Ploeger, A. Rap, B. Vogel, P. Konopka, M. Dameris, and P. Forster, 2012: Impact of uncertainties in atmospheric mixing on simulated UTLS composition and related radiative effects. *J. Geophys. Res.*, **117**, D16305, doi:10.1029/2012JD017751.

Shepherd, T. G., and C. McLandress, 2011: A robust mechanism for strengthening of the Brewer–Dobson circulation in response to climate change: Critical-layer control of subtropical wave breaking. *J. Atmos. Sci.*, **68**, 784–797, doi:10.1175/2010JAS3608.1.

Shuckburgh, E., and P. Haynes, 2003: Diagnosing transport and mixing using a tracer-based coordinate system. *Phys. Fluids*, **15**, 3342–3357, doi:10.1063/1.1610471.

——, W. Norton, A. Iwi, and P. Haynes, 2001: Influence of the quasi-biennial oscillation on isentropic transport and mixing in the tropics and subtropics. *J. Geophys. Res.*, **106**, 14 327–14 337, doi:10.1029/2000JD900664.

Tung, K. K., 1986: Nongeostrophic theory of zonally averaged circulation. Part I: Formulation. *J. Atmos. Sci.*, **43**, 2600–2618, doi:10.1175/1520-0469(1986)043<2600:NTOZAC>2.0.CO;2.

Wagner, R. E., and K. P. Bowman, 2000: Wavebreaking and mixing in the Northern Hemisphere summer stratosphere. *J. Geophys. Res.*, **105**, 24 799–24 807, doi:10.1029/2000JD900320.

Wallace, J. M., R. L. Panetta, and J. Estberg, 1993: Representation of the equatorial stratospheric quasi-biennial oscillation in EOF phase space. *J. Atmos. Sci.*, **50**, 1751–1762, doi:10.1175/1520-0469(1993)050<1751:ROTESQ>2.0.CO;2.

Waugh, D. W., and R. A. Plumb, 1994: Contour advection with surgery: A technique for investigating finescale structure in tracer transport. *J. Atmos. Sci.*, **51**, 530–540, doi:10.1175/1520-0469(1994)051<0530:CAWSAT>2.0.CO;2.

——, and L. M. Polvani, 2000: Climatology of intrusions into the tropical upper troposphere. *Geophys. Res. Lett.*, **27**, 3857–3860, doi:10.1029/2000GL012250.

——, R. A. Plumb, and L. M. Polvani, 1994: Nonlinear, barotropic response to a localized topographic forcing: Formation of a tropical surf zone and its effect on interhemispheric propagation. *J. Atmos. Sci.*, **51**, 1401–1416, doi:10.1175/1520-0469(1994)051<1401:NBRTAL>2.0.CO;2.

Webster, P. J., and J. R. Holton, 1982: Cross-equatorial response to middle-latitude forcing in a zonally varying basic state. *J. Atmos. Sci.*, **39**, 722–733, doi:10.1175/1520-0469(1982)039<0722:CERTML>2.0.CO;2.

Wheeler, M., and G. N. Kiladis, 1999: Convectively coupled equatorial waves: Analysis of clouds and temperature in the wavenumber–frequency domain. *J. Atmos. Sci.*, **56**, 374–399, doi:10.1175/1520-0469(1999)056<0374:CCEWAO>2.0.CO;2.

Wolter, K., and M. S. Timlin, 1998: Measuring the strength of ENSO—How does 1997/98 rank? *Weather*, **53**, 315–324, doi:10.1002/j.1477-8696.1998.tb06408.x.